Biotechnological Communication

BBRC Bioscience Biotechnology Research Communications

Biosc.Biotech.Res.Comm. Vol 13 (2) April-May-June 2020 Pp-676-682

# BiOCl Nano Pellets Preparation and their White/Solar Light Mediated Photocatalytic Activities Evaluation on Carbamate Pesticide Oxamyl and Synthetic Dye Azure B

Satish Piplode[1]*, Vinars Dawane[2], Vaishali Joshi[3] and Brijesh Pare[4]

[1]*Department of Chemistry, Govt. P G College Pipariya Hoshangabad MP India -461775*

[2]*School of Environment and Sustainable Development, Central University of Gujarat Gandhinagar Gujarat India- 382030*

[3]*Department of Chemistry, Govt. P G College Manawar Dhar M P India - 454446*

[4]*Department of Chemistry, Govt Madhav Science P G College Ujjain M P India- 456010*

## ABSTRACT

A quick, reliable, simple and one-pot sonochemical method has been discussed for the synthesis of BiOCl nanomaterial by using Bismuth Nitrate as a precursor along with HCl, Ammonia and L – lysine in water medium at 298.15 K under the designed and developed open glass double-walled beaker reactor. The nanomaterial was further characterized by using PSA, DLS, FTIR, BET, FT-RAMAN, Photoluminescence spectroscopy, HRXRD and HRFESEM. As a result, highly pure and well crystalline BiOCl nano pallets were obtained. HR-XRD results revealed their sizes between 40-50 nm followed by PSA, DLS and HRFESEM analysis. The prepared nanomaterial was tested for its photocatalytic activities under the designed and developed reactor on a carbamate pesticide Oxamyl and a synthetic dye Azure B under the white light lamp and solar light. Prepared BiOCl nanomaterial showed the impressive photocatalytic activity against pesticide under solar light only and able to degrade selected dye under both lights. Present results concludes a potential future utilization of BiOCl nanomaterial as great environmental remediation technology for various hazardous as well as persistent compounds removal.

**KEY WORDS:** BiOCI NANOMATERIAL, SYNTHESIS, CHARACTERIZATION, OXAMYL PESTICIDE, AZURE B DYE AND PHOTOCATALYSIS.

## INTRODUCTION

The Bismuth oxychloride has been extensively studied as an impressive material and a promising technology in the field of oxide-based semiconductors and heterogeneous catalytic degradation of various organic contaminants as well as environmental remediation purposes (Chen et al., 2010; Guerrero et al., 2014; Gao et al., 2018; Yang et al., 2018). BiOCl class of nanomaterials are very efficient photocatalytic semiconductor catalysts (Zhao et al., 2014) because of specific layered structures (Zhang et al., 2006), various 1 & 2-dimensional arrangements (Yang et al., 2019) and nanonetwork assemblies (Guo et al., 2018) viz. nanoflakes (Li et al., 2011), nanoflowers (Cheng et al., 2012), nanofibers (Zhang et al., 2016), nanowires (Wu et al., 2016), nanobelts (Wang et al., 2017), nanosheets (Shi et al., 2018) and several other self-similar micro (Mendez-Alvarado et al., 2020) - mesosphere structures (Guo et al., 2012; Xie et al., 2015; Ji et al.,

**Article Information:***

1/

2020) by a variety of reported synthesis methods including sonochemical (Geng et al., 2005), template-assisted routes (Wu et al., 2010), hydrolysis (Li et al., 2011), microwaves (He et al., 2015), hydrothermal synthesis (Hu et al., 2016) and biological/plant assisted (Garg et al., 2018; Yadav et al., 2019).

Over recent decades, due to simple synthesis, low cost, low toxicity, stability and ability to absorb UV as well as sunlight made BiOCl nanomaterials a preferential choice over other oxide based semiconductor materials like polyoxometalates (Mylonas et al., 1996), non-metallic doped $TiO_2$ (Asahi et al., 2001), complex oxides (Luan et al., 2009), $WO_3$ (Ashok kumar and Maruthamuthu, 1989; Li et al., 2012), as well as several other solar light-absorbing materials common nanomaterials like $TiO_2$ (Shaham-Waldmann and Paz, 2016; Lee et al., 2020). Thus the present study was an attempt to understand the synthesis, characterization and photocatalytic activity of BiOCl nanomaterial. The prepared BiOCl nanomaterial was further evaluated for its photocatalytic activity against a Carbamate pesticide Oxamyl (Fig.1B) and a synthetic dye Azure B (Fig. 1C) under visible and solar light.

Figure 1: A. – Prepared BiOCl nanomaterial power in a vial. B- The chemical structure of Oxymal pesticide. C – The chemical structure of Azure B dye. D – The open glass double walled beaker reactor.

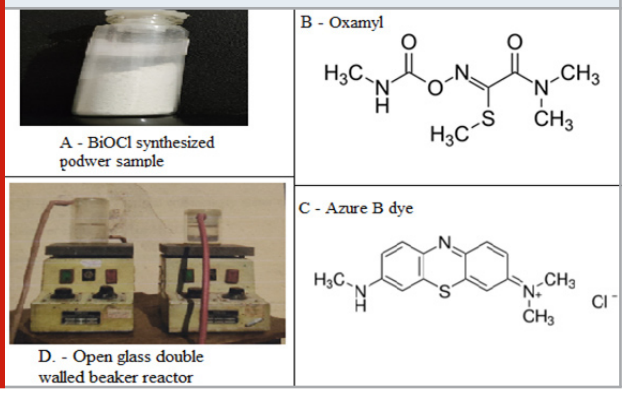


## MATERIAL AND METHODS

**Synthesis of BiOCl:** All of the reagents were analytical grade and commercially available. They were used without further purification. Milli-Q water (Millipore SAS 67/20 Mosheim) of $10^{-7}$S cm-1 was used for solution preparation. Typically, 10 mmol of Bi $(NO_3)3•5H_2O$ (4.85g) and 0.4 g of L-lysine was dissolved in concentrated HCl (dropwise). Then the mixture was quickly diluted to 100 mL by water for the immediate formation of precipitates. The solution was adjusted to pH = 9 by adding 5 wt. % ammonia solution, the BiOCl product was collected and washed with water and alcohol, (Chen et al 2013).

**Characterization methods:** Milli-Q water was used for solution preparation as well as setting black in PSA and DLS instruments. A pinch of (0.005 g) power was taken and 30 ml of water was added and sonicated for 30 minutes at 298.15 K. After that centrifugation performed at 7000 rpm for 15 minutes. The supernatant was used as a sample for particle size distribution analysis (Malvern Zetasizer Nano S90) and Dynamic light scattering analysis (MicrotracZetatrac, U2771). X-ray diffraction patterns (XRD) of the nanomaterial was recorded by D8 advance diffractometer (BRUKER). The structural information of nanomaterial was measured by a Fourier transform spectrophotometer (FT-IR, Bruker). The surface morphology of the sample was observed by using High-resolution field emission scanning electron microscope (Zeiss, model name SIGMA VP). Material scattering analysis carried out by FT RAMAN (BRUKER RFS 27 Model). Photoluminescence spectroscopy (Horiba Scientific) was used for the further electron structure elucidation of nanomaterial and specific surface area was calculated by BET analyser. The degradation studies were carried out in the designed and developed reactor by using UV-Vis spectrophotometer.

Measurement of Photocatalytic activity: Pesticide and dye solutions were freshly prepared by dissolving in Milli-Q water. An open glass double-walled beaker reactor was designed and developed to carry out a controlled degradation experiment (Fig. 1D). A space for continue water pump was present between the double-walled beaker to maintain the temperature during the whole experiment. A magnetic shaker was also added beneath the bottom of the double-walled beaker to insure uniform stirring on medium (Fig. 1D). Before light experiments, dark (adsorption) experiments were carried out to know the adsorption limit of pesticide or dye on the catalyst. For solar experiments, pesticide/dye solution of 100 mL was taken with the known amount of the catalyst. The solution was illuminated under bright visible/solar light. At specific time intervals, an aliquot (5 ml) of the mixture withdrawn and centrifuged for 2 minutes to remove the BiOCl particles. A PC based double beam spectrophotometer (Systronics – 2202) was used for measuring absorbance at different time intervals. The intensity of light was measured by a Lux meter (Lutron, LX-101). The pH and conductivity of the solution was constantly been monitored using a pH meter and conductivity meter. The efficiency of photocatalytic process was calculated as:

$$\%\,Efficiency = \frac{C_0 - C}{C_0}\ x\ 100$$

Where $C_0$ was the initial absorbance and C was the absorbance at different time intervals of photocatalytic process, (Sarwan et al 2014).

## RESULTS AND DISCUSSION

A one-pot sonochemical synthesis was performed by using Bismuth nitrate as Bi source. The dropwise HCl used as Cl – source in the medium. The basicity was maintained by addition of the 5 wt. % ammonia solution to restrict the medium pH at 9. The L lysine was used as surfactant or capping agent and water was used as the solvent. After the 10 minutes reaction, the centrifuged sample was dried in the lyophilizer and the white powder

used as a sample for further analysis and kept in the glass vial (Fig. 1A). The pinch of this powder sample was further used for PSA and DLS analysis to understand the size distribution. The PSA evaluation showed the average size of the nanomaterial between 44 nm – 46 nm in the intensity graph along with the Poly Disperse Index (PDI) was 0.326 detected (Fig.2).

Figure 2: The Particle size analyser results of BiOCl nanomaterial. A. - Showing the size distribution pattern according to the intensity. B. – the particle size analysis curves. C – The calculated Size, PDI, intercept and result quality report. D – The sample details and E – system details.

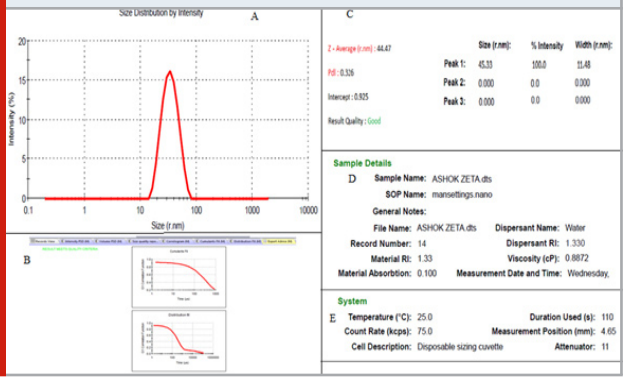


The Dynamic Light Scattering evaluation revealed the whole hydrodynamic volume measurement of water sample between 70 – 135 nm in different graphs of the same sample viz. area, intensity, volume and number graphs (Fig.3). The surface charge calculated was found to be negative and the zeta potential was detected – 18.22 mV (Fig. 3) showed strong stability of synthesized nanomaterial along with PDI of 0.371.

Figure 3: The DLS analysis of BiOCl nanomaterial. The Area, Intensity, volume and number graphs of same material. The Diameters and physicochemical analytic data of sample were present in tables associated and the 0.371 PDI was detected.

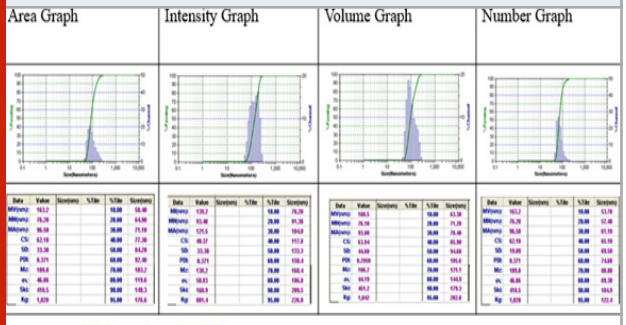


PDI was observed = 0.371

| Parameters | Diameter | Volume % | Width |
|---|---|---|---|
| Area | 84.20 | 100% | 66.60 |
| Intensity | 133.3 | 100% | 108.70 |
| Volume | 94.60 | 100% | 89.20 |
| Number | 69.50 | 100% | 38.20 |

| | |
|---|---|
| Zeta potential | - 18.22 mV |
| Conductivity | 15 uS/cm |
| Viscosity | 0.8620 cp |
| Mobility | -1.44 u/s/V/cm |
| Temperature | 299.3K |
| Dielectric cont. | 79 |

The XRD patterns of the BiOCl sample showed a well and high crystalline preparation of nanomaterial along with the reference of standard tetragonal structure (JCPDS 06-0249) and no other diffraction intense peaks were detected. The planes of material found to be in good arrangement regarding the unit cell of the tetragonal structure. The four important diffraction peaks viz. (110), (102), (101) and (200) were found to be prominent, intense and sharper while other peaks were relatively weak (Fig. 4).

Figure 4: The HR-XRD pattern of prepared BiOCl material. Where th 110, 102, 101 and 200 peaks where prominent.

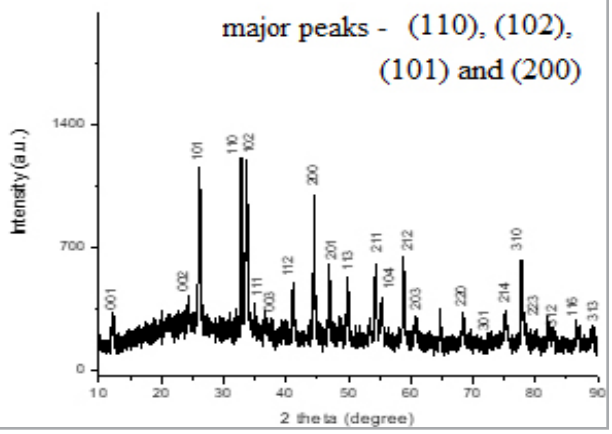


From the x-ray patterns, the broadening of the diffraction peaks of the nanomaterial was obvious. Which was characteristic of nanosized by applying Debye- Scherrer formula.

$$D = \frac{0.9\lambda}{\beta cos\theta}$$

Where D was the mean particle size, λ was the wavelength of incident X-ray (1.5406 ˚A), θ was the degree of the diffraction peak, and β was the full width at half maximum (FWHM) of the XRD peak appearing at the diffraction angle θ. The broadening of the absorption spectrum could be due to the quantum confinement of the nanoparticles. The mean calculated crystallite size was observed between 40 - 50 nm (Tab. 1).

Table1. Summary of XRD analysis for BiOCl nanomaterial.

| S.No. | 2 θ | plane | d spacing | Size (nm) |
|---|---|---|---|---|
| 1 | 26.103 | 101 | 0.173948 | 48 |
| 2 | 32.800 | 110 | 0.217488 | 45 |
| 3 | 33.560 | 102 | 0.222126 | 46 |
| 4 | 44.387 | 210 | 0.290926 | 49 |

The topological imaging of BiOCl nanomaterial was carried out with FE-SEM analysis. The surface electron

imaging showed many pallets like morphology of overall BiOCl material with a very smooth surface (Fig. 5A). The particle size obtained for PSA, DLS, XRD and FESEM analysis were found to be in good agreement with each other. These results have been found to be consistent with the literature (Baladi et al 2010). The elemental composition was also tested for BiOCl nanomaterial with the help of EDS analysis that revealed the clear detection of Bi, Cl and O in the sample (Fig. 5B & Tab.2).

**Figure 5: The surface morphological evaluation and elemental composition analysis of BiOCl. (A) HR-FESEM image of BiOCl and (B) EDS pattern of BiOCl.**

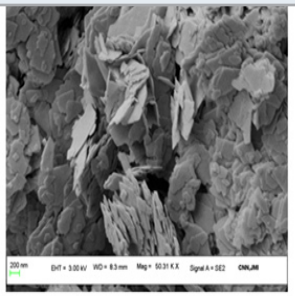

A . - FE SEM image of BiOCl material

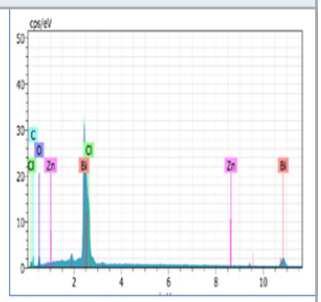


B . - EDS pattern graph of BiOCl material

FT-IR spectra functional group evaluation of BiOCl nanomaterial showed strong absorption bands at low-frequency zone (between, 400–600 $cm^{-1}$). These peaks were attributed to the Bi–O vibration of chemical bonds in the sample (Fig. 6A) and showed a good agreement with EDS results. (Chang et al 2014).

**Figure 6 Spectroscopic analysis of BiOCl. A - FT-IR spectra of the BiOCl and B. – Raman specta of BiOCl.**

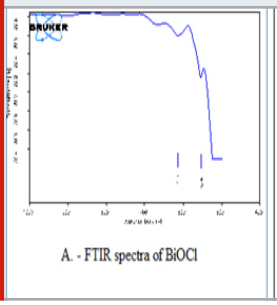


A. - FTIR spectra of BiOCl

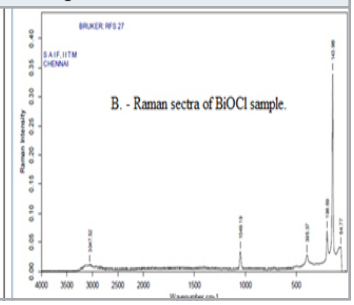


FT – Raman spectrum analysis was also carried out to assess the vibrational/ structural properties of the crystal. As XRD result indicated that the tetragonal structure of BiOCl belongs to the $P_4/nmm$ ($D^7_{4h}$) space group with

**Table 2. The EDS data of BiOCl nanomaterial.**

| El | AN | Series | unn. [wt.%] | C norm. [wt.%] | C Atom. C [wt.%] | Error (1 SIgma) | [wt.%] |
|---|---|---|---|---|---|---|---|
| Bi | 83 | L-series | 93.39 | 78.76 | 0.08 | 3.10 | |
| Cl | 17 | K-series | 11.26 | 9.50 | 18.40 | 0.41 | |
| O | 8 | K-series | 9.24 | 7.79 | 33.48 | 1.70 | |
| C | 6 | K-series | 4.59 | 3.87 | 22.13 | 0.91 | |
| Zn | 30 | K-series | 0.10 | 0.08 | 0.09 | 0.04 | |
| Total: | | | 118.58 | 100.00 | 100.00 | | |

two molecular formulae per unit cell. For this kind of structure, the correlation method indicated that the optical modes were as follows: $\Gamma = 2A_{1g} + 2A_{2u} + B_{1g} + 3E_g + 2E_u$, where the g modes were Raman-active only and u modes were infrared-active only. Raman spectra of the pallets like nano BiOCl material showed four bands at 64.77 $cm^{-1}$, 143.98 $cm^{-1}$, 198.69 $cm^{-1}$, 395.97 $cm^{-1}$ related to various type of vibrations and an agreement between XRD and Raman data of the sample (Fig. 6B). Same raman shift has been also observed by other authors (Davies 1973, Geng et al 2005 and Cao et al 2009).

The material further characterized for its photoluminescence spectra (Fig. 7A) and the results were elaborated along with original data and FFT data in visible light zone (Fig. 7B). The thick red curve was the fitted result of the originally scattered dots. The main emission peaks were observed in the visible light area at 597.5 nm and 627.5 nm indicated the orange emission and one more peak at 652.52 nm was also observed which was related to red emission (Fig. 7A-B). The main peak in Visible light region found to be ascribed to the band gap recombination of electron–hole pairs. That indicated the efficient photocatalytic activity in visible/solar light. (Duo et al 2015).

As photocatalytic properties also depend on the surface

**Figure 7: Photoluminescence spectroscopy spectra of BiOCl material (A) and the original data and FFT data in visible region (B).**

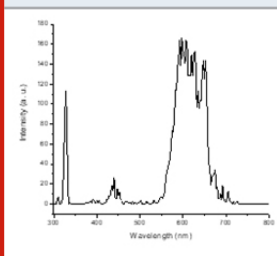


A. - Photoluminescence spectroscopy spectra of BiOCl material.

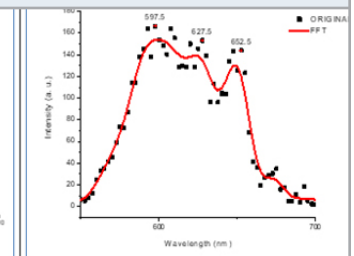


B. - The original data and FFT data in visible region

area of the catalyst so a Brunauer–Emmett–Teller (BET) analysis was carried out to determine the total surface area of the prepared catalysts (Tab. 3). In that analysis 21.591 $m^2/g$ surface area and 7.672 cc/g total pore

volume were observed. That showed a strong correlation along with good agreements with photocatalytic activity and degradation curve data of BiOCl nanomaterial with selected compounds.( Zhang et al 2015).

Table 3. The BET analysis results for BiOCl nanomaterial and summary of Average Pore Size, BJH adsorption, DFT method, BET

| Average Pore Size summary | |
|---|---|
| Average pore Radius | 7.10672 Å |
| BJH adsorption summary | |
| Surface Area | 3.096 m²/g |
| Pore Volume | 0.004 cc/g |
| Pore Radius Dv(r) | 16.709 Å |
| DFT method summary | |
| Surface Area | 11.011 m²/g |
| Pore Volume | 0.012 cc/g |
| BET summary | |
| Surface Area | 21.591 m²/g |
| Total Pore Volume | 7.672 cc/g |

**Photocatalytic studies and mechanism of degradation assessment:** The photocatalytic activities of nano BiOCl were evaluated with the degradation of Oxamyl pesticide (Fig. 1B) and Azure B dye (Fig.1C) in the presence of solar and visible light. For both pesticide and dye degradation experiments photolysis, adsorption and photocatalysis studies were carried out in the form of five experiments. The activities were calculated as $C/C_0$ versus time where C was the absorbance at a particular time and $C_0$ was the initial absorbance respectively. In Oxamyl degradation studies no significant results obtained in the photolysis and absorption phenomena. The degradation of Oxymyl pesticide was found to be very low under visible light as well as solar light in the absence of BiOCl nanomaterial. It was also observed that the degradation of pesticide was unable to initiate in the dark. The BiOCl mediated pesticide degradation initiated when light source applied. It was observed that visible light-mediated degradation was not showed the favourable response but solar light-mediated degradation showed impressive results. It may be possible because the solar light contained UV as well as visible light zone photons and UV light initiated the response and other electromagnetic energy photons favoured further reaction by inducing it in the combination (Fig. 8A).

Same experiment was performed for Azure B dye and approximately the same degradation patterns obtained in the photolysis and absorption phenomena. A major difference was that dye was also degraded to some extent in the presence of visible light. It was also observed that the dye was completely degraded in the presence of solar light because both UV and visible lights were present in solar light. Thus it can be assumed that UV light was responsible to initiate the photocatalysis reaction and solar light further propagated the degradation process. As a result, the photocatalytic degradation of Azure B dye using solar light was the favourable method to mineralise the dye solution and combination of UV and visible light was responsible to induce the process (Fig. 8B), ( Pare et al 2017).

Figure 8: The photcatalytic degradation of Oxamyl pesticide results (A) and Azure B dye degradation results (B). The Experimental condition for pesticide degradation studies: [Oxamyl] = $10^{-4}$ mol $dm^{-3}$, BiOCl NPs= 80mg/100ml, pH= 6.2. Experimental condition for dye degradation studies [Azure B] = 4.0 × $10^{-5}$ mol $L^{-1}$, BiOCl= 30 mg/100 mL pH = 8.0.

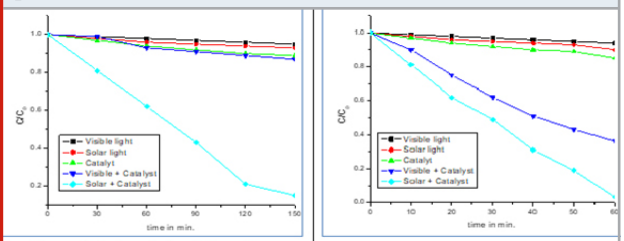


A. - Photcatalytic degradation of Oxamyl pesticide.

B. - Photocatalytic degraation of Azure B dve.

## CONCLUSION

A very simple, quick, facile and environmentally benign process for BiOCl nano pallets preparation at room temperature was discussed and highlighted in this work. Précised synthesis and various characterization results indicated the formation of remarkable BiOCl nanomaterial that was having sheet-like/ pallets structures at an eye-catching tiny size range. The generated nanomaterial found to be active as a potential photocatalyst capable to degrade carbamate pesticide Oxamyl as well as Azure B dye under the designed and developed open glass double-walled beaker reactor.

## ACKNOWLEDGMENTS

The authors are grateful to following institutions for extending various analytical instrumentation facilities, viz, centre for Nano science and Nanotechnology, JMI University New Delhi, Department of Pharmaceutical Chemistry, Govt. Madhav Science P G College Ujjain, SAIF, IIT Madras, SIC IIT Indore, CSS, IACS Kolkata and Central University Gujarat, Gandhinagar for library services. Dr. Satish Piplode and Vinars Dawane are thankful to UGC – New Delhi for financial assistance.

## REFERENCES

Asahi, R.Y.O.J.I., Morikawa, T.A.K.E.S.H.I., Ohwaki, T., Aoki, K. and Taga, Y., (2001). Visible-light photocatalysis in nitrogen-doped titanium oxides. Science, 293(5528), pp.269-271.

Ashok Kumar, M. and Maruthamuthu, P., (1989). Preparation and characterization of doped $WO_3$ photocatalyst powders. Journal of materials science, 24(6), pp.2135-2139.

Baladi A. and Sarraf Mamoory, R. (2010), Investigation of different liquid media and ablation times on pulsed

laser ablation synthesis of aluminum nanoparticles. Applied Surface Science, 256, (24), pp. 7559-7564.

Cao S., Guo C., Lv Y., Guo Y. and Liu Q. (2009) A novel BiOCl film with flowerlike hierarchical structures and its optical properties, Nanotechnology 20 pp 275702-09.

Chang F., Xie Y., Zhang J., Chen J., Li C., Wang J., Luo J., Deng B. and Hu X., (2014), Construction of exfoliated g-$C_3N_4$ nanosheets- BiOCl hybrids with enhanced photocatalytic performance, RSC Adv., 4, pp 28519-28528.

Chen L., Huang R., Xiong M., Yuan Q., He J., Jia J., Yao M.-Y., Luo S.-L., Au C.-T., and Yin S.-F. (2013) Room-Temperature Synthesis of Flower-Like BiOX (X=Cl, Br, I) Hierarchical Structures and Their Visible-Light Photocatalytic Activity. Inorg. Chem., 52, pp 11118–11125.

Chen, F., Liu, H., Bagwasi, S., Shen, X. and Zhang, J., (2010). Photocatalytic study of BiOCl for degradation of organic pollutants under UV irradiation. Journal of Photochemistry and Photobiology A: Chemistry, 215(1), pp.76-80.

Chen, L., Yin, S.F., Huang, R., Zhou, Y., Luo, S.L. and Au, C.T., (2012). Facile synthesis of BiOCl nano-flowers of narrow band gap and their visible-light-induced photocatalytic property. Catalysis Communications, 23, pp.54-57.

Davies J E D 1973 Solid state vibrational spectroscopy—III[1] The infrared and raman spectra of the bismuth(III) oxide halides J. Inorg. Nucl. Chem. 35 (5) 1531-1534

Duo F., Wang Y., Mao X., Zhang X., Wang Y. and Fan C., (2015). A $BiPO_4$/BiOCl heterojunction photocatalyst with enhanced electron-hole separation and excellent photocatalytic performance Appl. Surf. Sci., 340, pp 35–42

Gao, X., Peng, W., Tang, G., Guo, Q. and Luo, Y., (2018). Highly efficient and visible-light-driven BiOCl for photocatalytic degradation of carbamazepine. Journal of Alloys and Compounds, 757, pp.455-465.

Garg, S., Yadav, M., Chandra, A., Gahlawat, S., Ingole, P.P., Pap, Z. and Hernadi, K., (2018). Plant leaf extracts as photocatalytic activity tailoring agents for BiOCl towards environmental remediation. Ecotoxicology and environmental safety, 165, pp.357-366.

Geng, J., Hou, W.H., Lv, Y.N., Zhu, J.J. and Chen, H.Y., (2005). One-dimensional BiPO4 nanorods and two-dimensional BiOCl lamellae: fast low-temperature sonochemical synthesis, characterization, and growth mechanism. Inorganic Chemistry, 44(23), pp.8503-8509.

Guerrero, M., Altube, A., García-Lecina, E., Rossinyol, E., Baró, M.D., Pellicer, E. and Sort, J., (2014). Facile in situ synthesis of BiOCl nanoplates stacked to highly porous $TiO_2$: a synergistic combination for environmental remediation. ACS applied materials & interfaces, 6(16), pp.13994-14000.

Guo, C.F., Zhang, J., Tian, Y. and Liu, Q., (2012). A general strategy to superstructured networks and nested self-similar networks of bismuth compounds. ACS nano, 6(10), pp.8746-8752.

Guo, S.Q., Zhu, X.H., Zhang, H.J., Gu, B.C., Chen, W., Liu, L. and Alvarez, P.J., (2018). Improving photocatalytic water treatment through nanocrystal engineering: mesoporous nanosheet-assembled 3D BiOCl hierarchical nanostructures that induce unprecedented large vacancies. Environmental science & technology, 52(12), pp.6872-6880.

He, J., Wang, J., Liu, Y., Mirza, Z.A., Zhao, C. and Xiao, W., (2015). Microwave-assisted synthesis of BiOCl and its adsorption and photocatalytic activity. Ceramics International, 41(6), pp.8028-8033.

Hu, X., Xu, Y., Zhu, H., Hua, F. and Zhu, S., (2016). Controllable hydrothermal synthesis of BiOCl nanoplates with high exposed {001} facets. Materials Science in Semiconductor Processing, 41, pp.12-16.

Ji, Q., Xu, Z., Xiang, W., Wu, Y., Cheng, X., Xu, C., Qi, C., He, H., Hu, J., Yang, S. and Li, S., (2020). Enhancing the performance of pollution degradation through secondary self-assembled composite supramolecular heterojunction photocatalyst BiOCl/PDI under visible light irradiation. Chemosphere, p.126751.

Lee, J.C., Gopalan, A.I., Saianand, G., Lee, K.P. and Kim, W.J., (2020). Manganese and Graphene Included Titanium Dioxide Composite Nanowires: Fabrication, Characterization and Enhanced Photocatalytic Activities. Nanomaterials, 10(3), p.456.

Li, W., Li, J., Wang, X. and Chen, Q., (2012). Preparation and water-splitting photocatalytic behavior of S-doped WO3. Applied surface science, 263, pp.157-162.

Li, Y., Liu, J., Jiang, J. and Yu, J., (2011). UV-resistant superhydrophobic BiOCl nanoflake film by a room-temperature hydrolysis process. Dalton Transactions, 40(25), pp.6632-6634.

Luan, J., Pan, B., Paz, Y., Li, Y., Wu, X. and Zou, Z., (2009). Structural, photophysical and photocatalytic properties of new $Bi_2SbVO_7$ under visible light irradiation. Physical Chemistry Chemical Physics, 11(29), pp.6289-6298.

Mendez-Alvarado, L.N., Medina-Ramirez, A., Manriquez, J., Navarro-Mendoza, R., Fuentes-Ramirez, R. and Peralta-Hernandez, J.M., (2020). Synthesis of microspherical structures of bismuth oxychloride (BiOCl) towards the degradation of reactive orange 84 dye with sunlight. Materials Science in Semiconductor Processing, 114, p.105086.

Mylonas, A., Hiskia, A. and Papaconstantinou, E., (1996). Contribution to water purification using polyoxometalates. Aromatic derivatives, chloroacetic acids. Journal of Molecular Catalysis A: Chemical, 114(1-3), pp.191-200.

Pare B., Piplode S. and Joshi V., (2017) Solar light assisted photocatalytic degradation of hazardous and

highly water soluble pesticide methomyl using flower like nano BiOCl, International Journal of Scientific Research in Physics and Applied Sciences, 5(5), pp 5-11.

Sarwan B., Pare B. and Acharya A. D., (2014). Heterogeneous photocatalytic degradation of Nile Blue dye in aqueous BiOCl suspensions, Applied Surface Science. 301. pp 99-106.

Shaham-Waldmann, N. and Paz, Y., (2016). Away from TiO2: a critical minireview on the developing of new photocatalysts for degradation of contaminants in water. Materials Science in Semiconductor Processing, 42, pp.72-80.

Shi, Y., Xiong, X., Ding, S., Liu, X., Jiang, Q. and Hu, J., (2018). In-situ topotactic synthesis and photocatalytic activity of plate-like BiOCl/2D networks $Bi_2S_3$ heterostructures. Applied Catalysis B: Environmental, 220, pp.570-580.

Wang, C.Y., Zhang, X., Qiu, H.B., Wang, W.K., Huang, G.X., Jiang, J. and Yu, H.Q., (2017). Photocatalytic degradation of bisphenol A by oxygen-rich and highly visible-light responsive $Bi1_2O_{17}Cll_2$ nanobelts. Applied Catalysis B: Environmental, 200, pp.659-665.

Wu, S., Wang, C., Cui, Y., Wang, T., Huang, B., Zhang, X., Qin, X. and Brault, P., (2010). Synthesis and photocatalytic properties of BiOCl nanowire arrays. Materials Letters, 64(2), pp.115-118.

Xie, J., Cao, Y., Jia, D., Qin, H. and Liang, Z., (2015). Room-temperature solid-state synthesis of BiOCl hierarchical microspheres with nanoplates. Catalysis Communications, 69, pp.34-38.

Yadav, M., Garg, S., Chandra, A. and Hernadi, K., (2019). Immobilization of green BiOX (X= Cl, Br and I) photocatalysts on ceramic fibers for enhanced photocatalytic degradation of recalcitrant organic pollutants and efficient regeneration process. Ceramics International, 45(14), pp.17715-17722.

Yang, Y., Wu, M., Zhu, X., Xu, H., Ma, S., Zhi, Y., Xia, H., Liu, X., Pan, J., Tang, J.Y. and Chai, S.P., (2019). 2020 Roadmap on two-dimensional nanomaterials for environmental catalysis. Chinese Chemical Letters, 30(12), pp.2065-2088.

Yang, Y., Zhang, C., Lai, C., Zeng, G., Huang, D., Cheng, M., Wang, J., Chen, F., Zhou, C. and Xiong, W., (2018). BiOX (X= Cl, Br, I) photocatalytic nanomaterials: applications for fuels and environmental management. Advances in colloid and interface science, 254, pp.76-93.

Zhang L., Yuan X., Wang H., Chen X., Wu Z., Liu Y., Gu S., Jiang Q., and Zeng G.. (2015) Facile preparation of an $Ag/AgVO_3$/BiOCl composite and its enhanced photocatalytic behavior for methylene blue degradation RSC Adv.5, pp 98184.

Zhang, K.L., Liu, C.M., Huang, F.Q., Zheng, C. and Wang, W.D., (2006). Study of the electronic structure and photocatalytic activity of the BiOCl photocatalyst. Applied Catalysis B: Environmental, 68(3-4), pp.125-129.

Zhang, Y., Park, M., Kim, H.Y., Ding, B. and Park, S.J., (2016). In-situ synthesis of nanofibers with various ratios of $BiOCl_x/BiOBr_y/BiOI_z$ for effective trichloroethylene photocatalytic degradation. Applied Surface Science, 384, pp.192-199.

Zhao, H., Tian, F., Wang, R. and Chen, R., (2014). A review on bismuth-related nanomaterials for photocatalysis. Reviews in Advanced Sciences and Engineering, 3(1), pp.3-27.